PROCEEDINGS OF SCIENCE

Performance of the ATLAS Pixel Detector at the Start of LHC Run 3

Marco Battaglia[a,*] **on behalf of the ATLAS Pixel collaboration**

[a] *University of California at Santa Cruz*
Santa Cruz Institute for Particle Physics,
1156 High Street, Santa Cruz, CA 95064, USA

E-mail: marco.battaglia@ucsc.edu

This contribution presents a characterisation of the ATLAS Pixel detector response obtained from the analysis of pp collisions recorded by the ATLAS detector at the LHC during Run 2 and at the start of Run 3. The effects of radiation damage are discussed in detail and compared to predictions from simulation accounting for non-ionising radiation damage effects to the pixel sensors.

ATL-INDET-PROC-2023-001
28 February 2023

10th International Workshop on Semiconductor Pixel Detectors for Particles and Imaging (Pixel2022)
12-16 December 2022
Santa Fe, New Mexico, USA

*Speaker

PoS(Pixel2022)006

1. Introduction

The Pixel detector [1] is the ATLAS detector [2] system installed closest to the LHC interaction region. It consists of four barrel layers and three forward disks on either side of the interaction region. The innermost layer (IBL) [3], installed in the shutdown period preceding the start of Run 2, is located at 3.3 cm from the beam axis and equipped with 200 µm-thick n^+-in-n planar and 230 µm-thick n^+-in-p 3D sensors with a 50×250 µm^2 pitch read out by FE-I4 front-end (FE) chips in 130 nm CMOS with 4-bit time-over-threshold (ToT) analog information for collected charge. All other barrel layers and the disks are equipped with 250 µm-thick n^+-in-n planar sensors with 50×400 µm^2 pitch and are read out by FE-I3 chips in 0.25 µm CMOS with 8-bit ToT analog information.

The Pixel detector determines the charged particle track extrapolation to the production vertex, it provides space points for the reconstruction of very low momentum particle tracks and it measures the charged particle specific energy loss, dE/dx, essential in the searches for anomalously ionising new particles.

The start of LHC Run 3 has brought the highest energy pp collisions delivered so far. The luminosity integrated at 13.6 TeV is expected to triple the ATLAS data set available for physics analysis by the end of 2025. But Run 3 is not only characterised by the large data set at high energy, the fluxes of particle emerging from the interaction region induce significant radiation damage effects in the detectors, in particular those located closest to the colliding beams [4]. With 200 fb^{-1} of integrated luminosity already delivered since 2015, the IBL sensors have received a particle fluence in excess of 10^{15} in units of 1 MeV neutron equivalent/cm^2. That will increase by more than a factor of two by the end of Run 3. At that point, sensors on all pixel layers will have reached, or exceeded, their design fluence limit. Therefore, radiation damage has become a parameter of relevance in evaluating the performance of the ATLAS Pixel system and of all the derived physics objects, in particular tracking and vertexing, in event reconstruction and physics analysis.

This contribution summarises the current results from the study of the ATLAS Pixel detector response at the start of Run 3, with special attention to their relation to radiation damage effects.

2. Pixel Radiation Damage

Of the various effects induced by radiation on the pixel detectors, displacement damage to the Si detector bulk is the most important effect. In fact, it is responsible for the decrease in collected charge yield and the increase in leakage current and depletion voltage. The particle fluence, Φ, responsible for Si bulk damage, on the pixel layers has been determined from the measured increase in leakage current, I_{leakage}, in the sensors. Since $I_{\text{leakage}} \propto \Phi$, measurements performed on the modules of the four barrel layers and modules groups along each detector stave of a single layer provide a mapping of the fluence along both the radial and longitudinal position of the pixel sensors [5], with annealing effects modelled using the "Hamburg model" [7]. Results are shown in Figure 1 in terms of the measured IBL leakage current in module groups along z and the rate of particle fluence on all barrel layers in units of 1 MeV n-eq/cm^2 per fb^{-1} of LHC delivered luminosity. One of the most striking features of this measurement is the enhanced fluence dependence on the longitudinal position on the two innermost pixel layers (IBL and B-Layer) compared to the simulation predictions, based on

Pythia 8 [8] for particle generation and FLUKA [9] or Geant 4 [10] for particle transport. Its origin is under investigation.

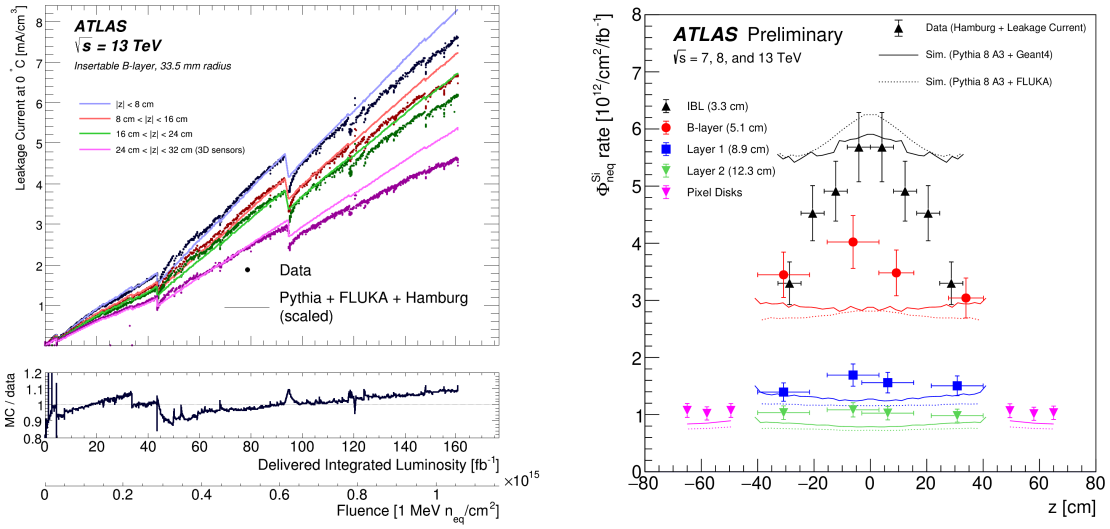

Figure 1: Particle fluence determination: (Left) Measured and predicted leakage currents for IBL sensors for four module groups spanning four regions along the longitudinal coordinate z. Modules in the highest $|z|$ region use 3D sensors (from [5]). (Right) The luminosity-to-fluence conversion factors for the barrel pixel layers as a function of the longitudinal coordinate, z, compared with the Pythia 8+FLUKA and Pythia 8+Geant 4 predictions. The error bars are dominated by the residual dependence of the leakage current on the high voltage past full sensor depletion, for the IBL, and by uncertainties on the power supply, temperature and luminosity, for the outer layers. Uncertainties on the silicon damage factors, relevant for the simulation and the Hamburg model, are not included (from [6]).

ATLAS has developed a radiation damage simulation based on realistic maps of the electric field across the Si bulk depth at different values of particle fluence and detector reverse bias voltage [11]. A custom radiation damage digitiser calculates the signals induced on the read-out nodes by charge carriers produced from the ionising particle energy losses, modelled using the Bichsel model [12]. The fluence-dependent electric field maps, Lorentz angles and weighting potentials used in the digitiser are all based on inputs derived from TCAD simulation [13].

The reduction of the collected signal amplitude in irradiated pixel sensors is due in part to the deformations of the electric field and in part to the formation of defects in the silicon lattice. These defects can trap charge carriers created by ionising particles. Trapping phenomena can be parametrised in terms of a charge carrier trapping time, τ, inversely proportional to the fluence, Φ. Trapped charge is also responsible for the change in shape of the electric field across the sensor thickness, with a region of low field developing in the central section of the active bulk, as fluence increases. The trapping rate ($1/\tau_e$) for electrons, indicated by simulation as the responsible for the majority of the collected charge, has been estimated using the data collected on IBL sensors during the bias voltage scan perfomed at the beginning of Run 3 in 2022. Fits to the cluster charge and to the slope of the increase of this charge with the applied bias voltage (HV) above the point of depletion give results in good agreement with the values used in the radiation damage digitiser, based on previous measurements [14–16]. The evolution of the computed electric field profile and

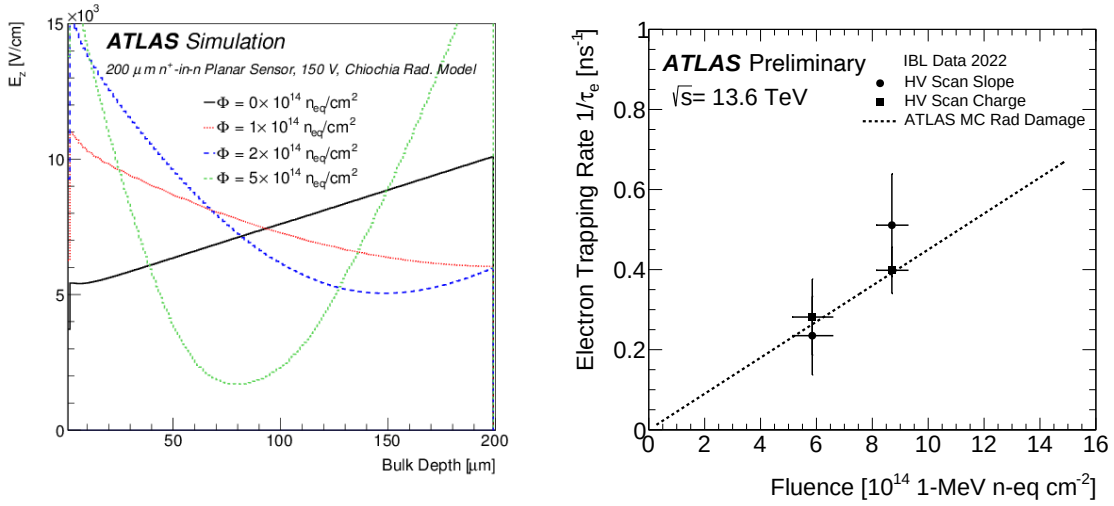

Figure 2: Radiation damage charge loss simulation: (Left) Simulated electric field magnitude along the Si bulk depth for an IBL planar sensor biased at 150 V for various fluences reached during Run 2 (from [11]). (Right) Electron trapping rate ($1/\tau_e$) estimated from fits to the cluster charge (filled squares) and to the slope of the cluster charge increase with the applied bias voltage above depletion (filled circles) as a function of the fluence on IBL sensors. The points at lower fluence are obtained using the 3D sensors installed at the end of the staves and those at higher fluence using the planar sensors in the centre of the staves. The dashed line shows the values used in the ATLAS radiation damage simulation for comparison (from [17]).

the measured trapping rate with the fluence is shown in Figure 2.

Given the importance of these effects on the IBL and B-Layer charge collection, the pixel radiation damage digitiser has been adopted by ATLAS in the official simulation for all the Run 3 Monte Carlo (MC) samples. As fluence grows with delivered integrated luminosity, E-field maps

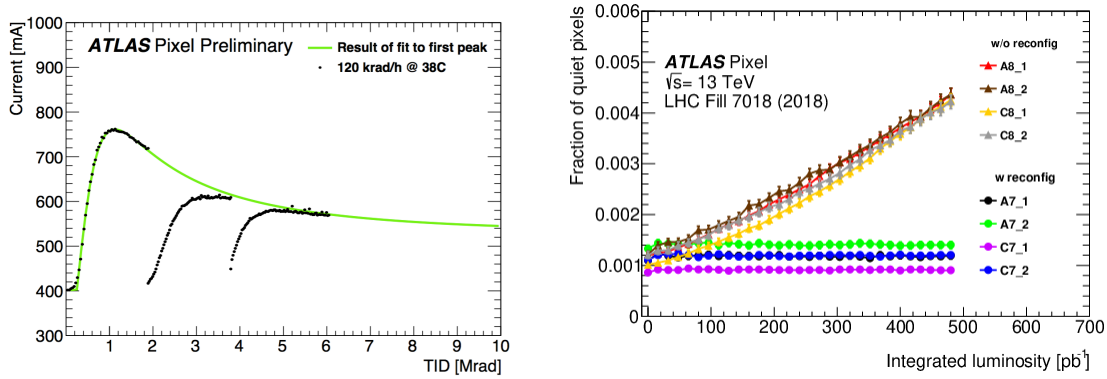

Figure 3: Radiation damage effects: (Left) Increase in current consumption of a single FE-I4 chip in data taking condition as a function of the total ionising dose (TID). The dose rate of 120 krad/h was delivered with an X-ray machine. After reaching the maximum of each peak the chip was annealed several hours resulting in the observed partial recovery (from [18]). (Right) Fraction of silent pixels due to SEU effects as a function of the integrated luminosity in LHC fill 7018 taken in 2018. Data are shown for the eight 3D IBL η rings with and without pixel register reconfiguration (from [19]).

and predictions are updated. Run 3 simulation uses four different predictions corresponding to fluences and pixel operating parameters for each year of data taking. The main uncertainties on the predictions in terms of collected charge are due to the conversion of the integrated luminosity to the *n*-eq fluence on the sensor and the electron trapping rate.

Besides Si bulk damage, other radiation effects are also relevant for the operation and performance of the detector. The total ionising dose (TID) surface effects on the FE chips induce transistor current variations (see left panel of Figure 3) that impact the ToT and threshold tunings on IBL and need to be carefully monitored and compensated by regular re-calibrations throughout the run period. Single Event Upset (SEU) and Single Event Transient (SET) affect the IBL FE global registers and the settings for individual pixels causing occupancy losses, noisy and silent pixels during data taking. SEU and SET effects have been studied in detail for the IBL FE-I4 chips [19]. Mitigation through reconfiguration of pixel registers during the LHC runs was tested in 2018 and the results are summarised in the right panel of Figure 3.

3. Pixel Detector Performance at the Start of Run 3

The modifications of the charge collection properties are the main effects of bulk radiation damage and show up conspicuously in the ATLAS pixel response, in particular that of the IBL and B-layer, as shown in Figure 4. The pixel performance assessment at the end of Run 2 and start of Run 3 has investigated detailed indicators of pixel response from cluster charge distribution to their variation with pixel bias voltage and charge collection efficiency as a function of fluence and depth of charge generation. These are important for determining the detector performance in terms of pixel hit efficiency and spatial resolution, most relevant for the performance of the derived physics objects. The comparison of results from data to the predictions from radiation damage

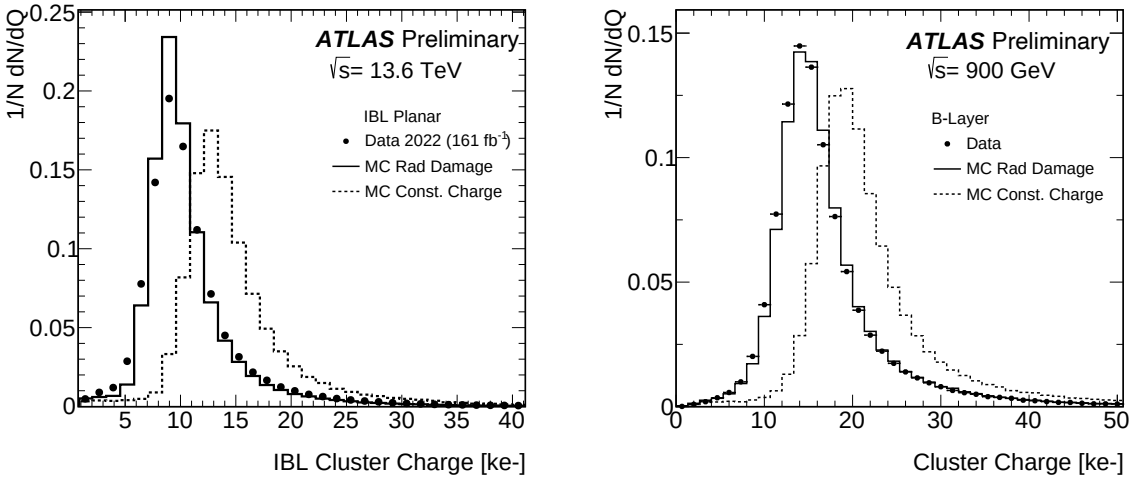

Figure 4: Pixel cluster charge corrected by the particle path in the Si for IBL (from [17]) (left) and B-Layer (from [20]) (right) planar sensors for clusters associated to reconstructed particle tracks. Points represent data at the beginning of the Run 3 in 2022, the histograms the MC predictions obtained with radiation damage (continuous line histogram) and constant charge (dashed line histogram) simulation.

simulation provides a validation of the new radiation damage MC framework. Figure 4 compares

the distribution of the charge in clusters on the IBL and B-Layer associated to reconstructed particle tracks in data collected at the beginning of Run 3 after ≃161 (191) fb^{-1} on the IBL (B-Layer) to the predictions of two simulation setups, one including radiation damage effects and one assuming constant charge collection. This comparison highlights the amount of charge loss in the sensors on the two innermost layer and the realistic description of these losses by the radiation damage simulation. The quality of these simulation predictions has been tested over the full period of IBL operation spanning from 2015 to the end of 2022 by comparing the simulated charge collection efficiency to that of measured for data. The cluster charge is characterised by the most probable value (MPV) of a Landau function folded with a Gaussian term used to model the cluster charge distributions. These are fitted to the measured and predicted distributions of charge for clusters associated to reconstructed tracks, corrected by the length of the track traversing the Si sensor bulk. The charge collection efficiency is defined in data as the ratio of the value measured at a given LHC integrated delivered luminosity to that measured at the start of detector operation, corresponding to the beginning of Run 2 for IBL. In simulation, this efficiency is computed as the ratio of the MPV measured on a sample simulated at the corresponding fluence value to that for a sample at zero fluence. Results are shown in Figure 5 and demonstrate a good agreement of simulation and data over two orders of magnitude of fluence. The fluence values used in the simulation are obtained

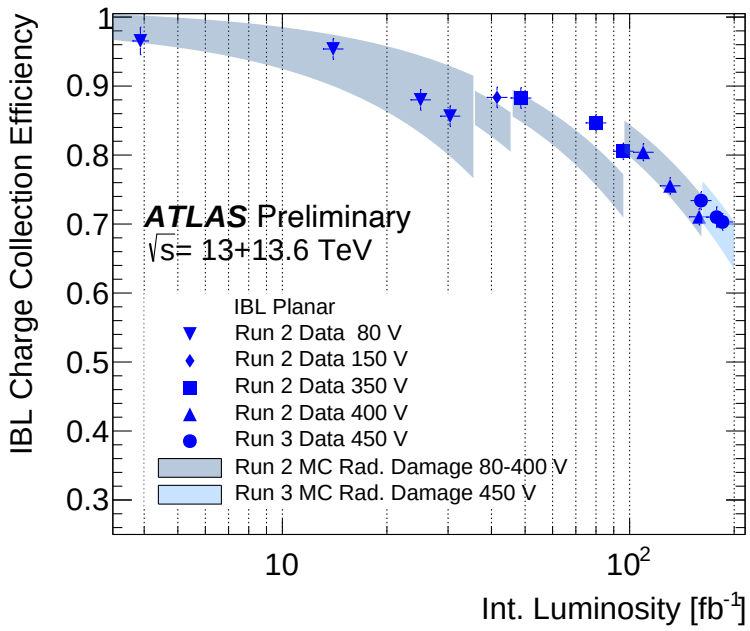

Figure 5: Charge collection efficiency as a function of the integrated delivered luminosity for IBL planar sensors for data and the ATLAS radiation damage simulation from the beginning of Run 2. The points represent the data and the bands the simulation predictions with their uncertainties. Sudden increases in charge collection efficiency at the beginning of each year are due to changes in the operational parameters (bias voltage and thresholds). In Run 2 the bias voltage was increased in steps from 80V in 2015 to 400V in 2018. In Run 3 the bias voltage was 450V in 2022 (from [17]).

from the integrated delivered luminosity and the conversion values extracted from the study of the detector leakage current shown in Figure 1, weighted over the longitudinal coordinate according to

the observed distribution of the longitudinal position, z, of IBL hits associated to the tracks selected in the analysis. The simulation uncertainty, defining the width of the error band, includes variations in the radiation damage model parameters as well as the uncertainty of the luminosity-to-fluence conversion.

While the total amount of collected charge in clusters is crucial for understanding changes in efficiency and spatial resolution, there are interesting correlations of charge collection that account for non-uniformity and bias effects appearing in the data. These shed light on radiation damage effects and validate details of the radiation damage simulation.

The first of these correlations is with the detector reverse bias voltage. The left panel of Figure 6 compares the evolution of the collected charge in the IBL with the applied voltage in data and simulation for the fluence conditions at the beginning of Run 3. The estimated depletion voltage is ∼230 V in both data and simulation. It is interesting to observe that the amount of collected charge in the damaged Si bulk continues to increase for voltages above this value due to the reduction of the charge trapping effect with the increasing charge carrier velocity. The simulation models this behaviour fairly well, thus confirming that the trapping constant used in the radiation damage digitiser is in agreement with the present data, as discussed in section 2 and shown in Figure 2.

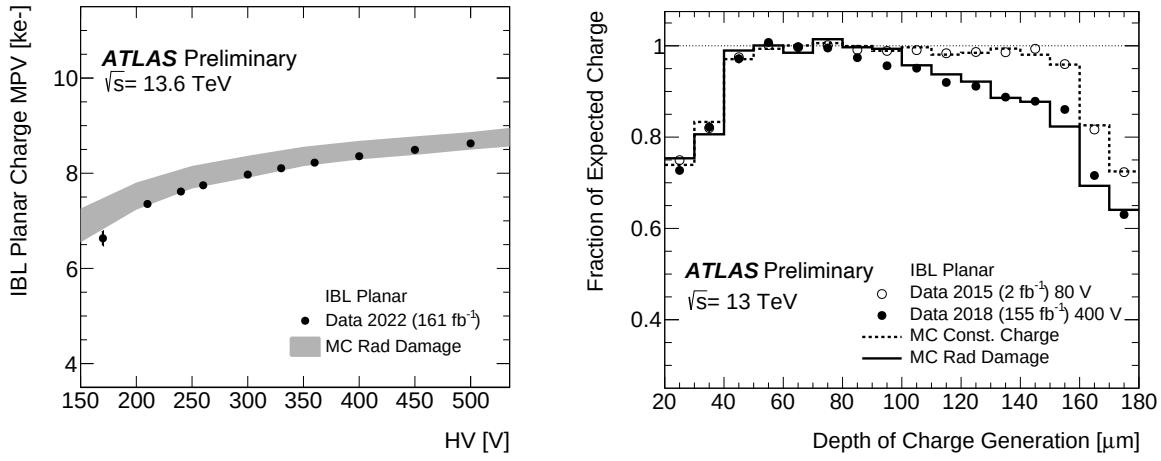

Figure 6: Charge collection properties: (Left) Pixel cluster most probable value (MPV) of the charge corrected by the particle path in the Si for IBL planar sensors for clusters associated to reconstructed particle tracks as a function of the detector bias voltage (HV). Points represent data recorded during an HV scan at the beginning of the Run 3 in 2022 (161 fb^{-1} of integrated luminosity), the grey band the MC prediction obtained with radiation damage simulation. The width of band represents the estimated uncertainty, dominated by that on the conversion of the integrated luminosity to the fluence on the sensor surface (from [17]). (Right) Charge collection efficiency as a function of the estimated depth of charge generation for IBL planar sensors in data, start of Run 2 in 2015 (2 fb^{-1} of integrated luminosity) shown by the open points and end of Run 2 in 2018 (155 fb^{-1} of integrated luminosity) by the filled points, and radiation damage simulation for matching fluence conditions. The drops observed at the two ends of the substrate thickness are due to resolution effects. In order to reduce these effects, only tracks with p_{T} >3 GeV and at least three pixels in the longitudinal projection are considered (from [17]).

The loss of charge yield at low values of the bias voltage shown in the left panel of Figure 6 is indicative of the incomplete charge collection through the sensor thickness. This efficiency can be

computed by comparing the fraction of the cluster charge deposited on the pixels ordered from the extrapolated point of track entrance in the Si substrate to that of exit in the longitudinal projection. For inclined tracks this pixel ordering corresponds to slices of the average depth of the track segment below the corresponding pixel readout nodes. The resulting scan of the fraction of the expected IBL charge as a function of the depth of charge generation is shown in the right panel of Figure 6 for data collected at the beginning and end of Run 2, compared to radiation damage simulation at the corresponding values of bias voltage and fluence. The response as a function of the depth of charge generation, flat for an unirradiated detector, develops a significant inefficiency for charge produced at large depth with increasing particle fluence due to trapping and electric field distortion effects. This inefficiency is precisely modelled by the radiation damage simulation.

The non-uniformity in charge collection induces biases in the pixel position for inclined tracks. These biases on data are corrected by alignment with tracks, sensitive to time-dependent effects [21]. With the use of radiation damage MC samples, the degradation of performance is not only modelled but it can also be mitigated using radiation damage-aware training and tuning of pixel and track reconstruction algorithms. This partially recovers performance loss due to charge collection inefficiencies and corrects for distortions due to charge collection dishomogeneities.

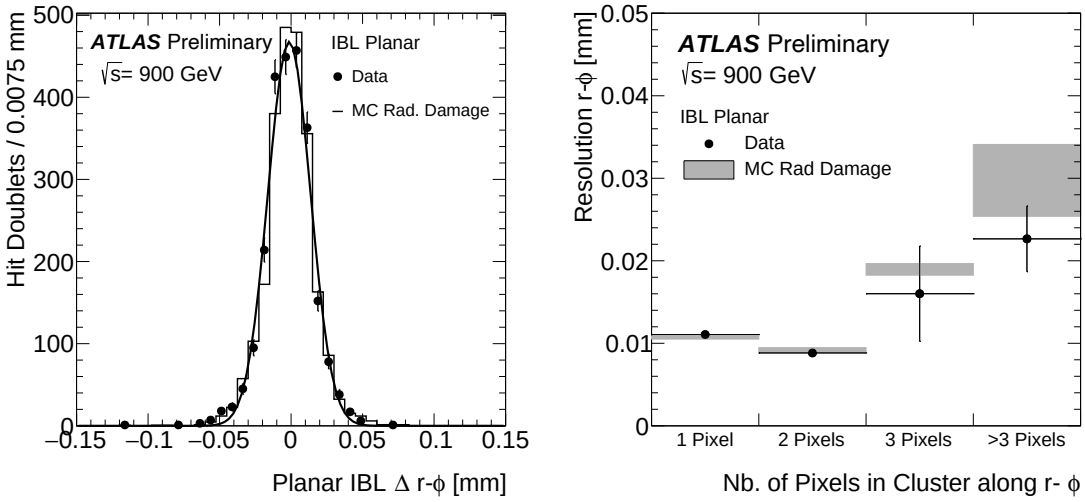

Figure 7: IBL spatial resolution: (Left) Difference between the corrected positions in the $r-\phi$ (50 µm pixel pitch) projection for reconstructed IBL hits on track in the overlap region. The distributions are obtained from samples of reconstructed particle tracks traversing the overlapping IBL modules and having two IBL hits associated, $|\eta| < 2$ for $r-\phi$ and < 1 for z, in 900 GeV collision events (filled circles with errors bars) and simulation (histogram). The curves represent the Gaussian fit to data (from [20]). (Right) Measured IBL hit resolution in the $r-\phi$ projection, $\sigma_{r-\phi}$, as a function of the cluster width along ϕ in early Run 3 collision events (filled circles with errors bars) and radiation damage simulation (open circles) (from [20]).

Pixel hit-on-track efficiency drives the uniformity of performance of tracking and derived physics objects as a function of the period at which data were recorded. The regular optimisation of operating bias voltages and thresholds ensures a uniform response of pixel clusters in terms of their hit-on-track efficiency. Overall, the drop in efficiency measured from start to end of Run 2 has been seen to be below 1% on all layers. This efficiency must be preserved in pixel operations under

challenging LHC Run 3 conditions, including the increase of the pile-up levels, inducing module de-synchronisations and readout bandwidth limitations.

The Pixel detector spatial resolution degrades with the collected charge loss, due to radiation damage effects. However, the impact of these effects on the resolution is modest, since the pixel hit position in multi-pixel clusters depends on relative quantities, namely the fraction of cluster charge shared between neighbouring pixels. This degradation is modelled using the radiation damage MC, which predicts a ~25% increase in the spatial resolution over a decade of operations, from start of Run 2 operation in 2015 to end of Run 3 in 2025, if the same algorithm and training is used. Significant mitigation to this increase is provided by the improvement in resolution obtained by using a Mixed Density Network (MDN) in the calculation of the cluster hit position and its training on radiation damage simulation samples [20].

The IBL sensor spatial resolution can be extracted from the correlation of the positions of hits on track reconstructed in the active region of adjacent modules overlaps in ϕ, where particles generate clusters on the two neighbouring modules. The distributions of the corrected position differences, $\Delta r - \phi$ and Δz, have widths proportional to the resolutions, $\sigma_{r-\phi}$ and σ_z, and depend only weakly on reconstructed track parameters and detector alignment [20, 22] (see Figure 7). Data taken in early 2022 are compared to simulation by measuring the spatial resolution along the small pixel pitch coordinate as a function of the number of pixels in the cluster along $r - \phi$ in the right panel of Figure 7. The spatial resolution for data agrees with the radiation damage simulation

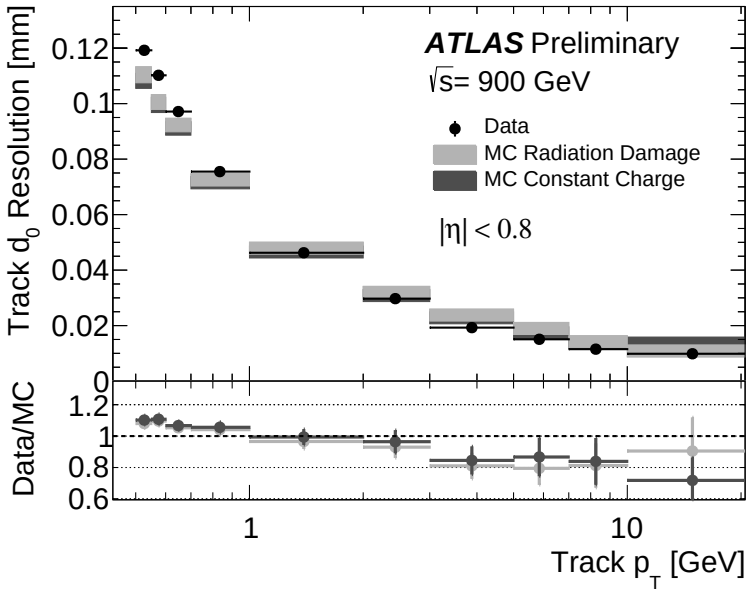

Figure 8: Unfolded transverse track extrapolation resolution as a function of the track p_{T} for $|\eta|$ <0.8 for early Run 3 data and the predictions of radiation damage and constant charge simulation. The lower panel shows the ratio of the resolution measured in data to the MC predictions. The uncertainties associated to the MC points account for statistics and the difference between the resolution values obtained with the residual and the unfolding methods (from [20]).

predictions. For comparison, constant charge simulation yields spatial resolution values that are

lower by ≃5% in both coordinates [20], compared to those predictions, when MDN trainings on MC samples generated with the corresponding fluence are used.

Finally, it is interesting to connect the performance of the IBL to that of particle track resolution. Owing to its position closest to LHC interaction region and the reduced pitch in z (250 μm compared to 400 μm for the other layers), the IBL carries the largest weight in determining the extrapolation of low-to-moderate p_{T} particles tracks to the primary vertex. This extrapolation resolution has been measured in the transverse plane as a function of the track p_T using the first Run 3 data and compared to MC samples obtained with and without the inclusion of radiation damage effects.

The resolution is measured as the Gaussian r.m.s. extracted from an iterative fit on the central portion of the unfolded transverse impact parameter, d_0, peak contained within a $\pm 1.5\sigma$ interval centred at the maximum value of the distribution. Results are given in Figure 8. The agreement between data and simulation is rather good and the measured impact parameter resolution is close to that obtained with 13 TeV collision data at the start of Run 2 [20]. The predictions by the radiation damage and the constant charge MC setups are also close, to underline the limited impact of radiation damage effects on the tracking performance for the fluence integrated so far by the ATLAS Pixel detector despite the significant changes in charge collection properties.

4. Conclusions

The ATLAS Pixel detector started Run 3 operations with parameters optimised to mitigate effects of radiation damage and boost tracking performance. ATLAS simulation includes a new radiation damage pixel digitiser accounting for detailed radiation effects in the Si bulk. This simulation is used to understand and predict impact of radiation damage on pixel response and also to understand their effect on physics objects used in physics analyses. The efficiency for pixel hit on track has been kept constant thanks to the increase of bias voltages and decrease of analog thresholds on the innermost layers. A novel Mixture Density Network trained on simulated samples generated with radiation damage MC and used for determining the spatial position of pixel hits in track reconstruction provides improved performance compared to Run 2, offsetting radiation damage effects on spatial resolution. The new radiation damage MC gives very good description of the pixel response down to details of charge collection properties. In track reconstruction, where radiation damage effects are still tiny, the Run 3 pixel operational parameters and adoption of new MDN has made it possible to achieve performance improvements compared to end of Run 2. ATLAS Pixels have just concluded a successful run of operation both in terms of their performance for physics and of the understanding and modelling of radiation damage effects. With the LHC high luminosity program setting an even higher target in terms of detector resistance to radiation damage and the pixel detector of the new ATLAS Inner Tracker (ITk) system [23] currently under construction, the lessons learned with the present Pixel detector in Run 3 are of crucial importance for the longer term future.

References

[1] G. Aad *et al.*, *ATLAS pixel detector electronics and sensors*, *JINST* **3** (2008), P07007.

[2] ATLAS Collaboration, *The ATLAS Experiment at the CERN Large Hadron Collider*, *JINST* **3** (2008), S08003.

[3] ATLAS IBL Collaboration, *Production and Integration of the ATLAS Insertable B-Layer*, *JINST* **13** (2018), T05008.

[4] I. Dawson (editor), *Radiation effects in the LHC experiments: Impact on detector performance and operation*, CERN-2021-001.

[5] ATLAS Collaboration, *Measurements of sensor radiation damage in the ATLAS inner detector using leakage currents*, *JINST* **16** (2021), P08025.

[6] ATLAS Collaboration, *Sensor Radiation Damage in the ATLAS Inner Detector using Leakage Currents*, ATLAS-IDET-2020-001.

[7] M. Moll, *Radiation damage in silicon particle detectors: Microscopic defects and macroscopic properties*, DESY-THESIS-1999-040.

[8] C. Bierlich *et al.*, *A comprehensive guide to the physics and usage of PYTHIA 8.3*, *Comput. Phys. Commun.* **191** (2015), 159.

[9] A. Ferrari *et al.*, *FLUKA: A multi-particle transport code*, SLAC-R-773 (2005).

[10] S. Agostinelli *et al.*, *Geant4 — a simulation toolkit*, *Nucl. Instrum. Meth. A* **506** (2003), 250.

[11] ATLAS Collaboration, *Modelling radiation damage to pixel sensors in the ATLAS detector*, *JINST* **14** (2019), P06012.

[12] H. Bichsel, *Straggling in thin silicon detectors*, *Rev. Mod. Phys.* **60** (1988), 663.

[13] V. Chiochia *et al.*, *Simulation of heavily irradiated silicon pixel sensors and comparison with test beam measurements*, *IEEE Transactions on Nuclear Science* **52** (4) (2005), 1067.

[14] G. Kramberger *et al.*, *Determination of effective trapping times for electrons and holes in irradiated silicon*, *Nucl. Instr. and Meth. A* **476** (2002), 645.

[15] G. Alimonti *et al.*, *A study of charge trapping in irradiated silicon with test beam data*, ATL-INDET-2003-014.

[16] CMS Collaboration, *Trapping in proton irradiated p+-n-n+ silicon sensors at fluences anticipated at the HL-LHC outer tracker*, *JINST* **11** (2016), P04023.

[17] ATLAS Collaboration, *Modelling of ATLAS IBL pixel response with radiation damage simulation*, ATL-INDET-INT-2022-002.

[18] ATLAS Collaboration, *Results from the ATLAS IBL low voltage current task force X-ray irradiation campaigns*, ATLAS-PIX-2015-008.

[19] G. Balbi *et al.*, *Measurements of Single Event Upset in ATLAS IBL*, *JINST* **15** (2020), P06023.

[20] ATLAS Collaboration, *Performance of ATLAS Pixel Detector and Track Reconstruction at the start of Run 3 in LHC Collisions at $\sqrt{s}$=900 GeV*, ATL-PHYS-PUB-2022-033.

[21] ATLAS Collaboration, *Alignment of the ATLAS Inner Detector in Run 2*, *Eur. Phys. J. C* **80** (2020), 1194.

[22] ATLAS Collaboration, *Efficiency and Hit Spatial Resolution of ATLAS IBL Sensors in LHC Run 2 Collision Events*, ATL-INDET-PUB-2016-001.

[23] ATLAS Collaboration, *Technical Design Report for the ATLAS Inner Tracker Pixel Detector*, CERN-LHCC-2017-021, ATLAS-TDR-030.